Front. Biol. 2017, 12(2): 124–138
DOI 10.1007/s11515-017-1447-1

RESEARCH ARTICLE

The radial organization of neuronal primary cilia is acutely disrupted by seizure and ischemic brain injury

Gregory W. Kirschen[1,2,3], Hanxiao Liu[3], Tracy Lang[3,4], Xuelin Liang[3], Shaoyu Ge[3], Qiaojie Xiong (✉)[3]

[1] *Medical Scientist Training Program (MSTP), Stony Brook University, Stony Brook, NY 11794, USA*
[2] *Molecular & Cellular Pharmacology Program, Stony Brook University, Stony Brook, NY 11794, USA*
[3] *Department of Neurobiology & Behavior, Stony Brook University, Stony Brook, NY 11794, USA*
[4] *Simons Summer Research Program (SSRP)*

BACKGROUND: Neuronal primary cilia are sensory organelles that are critically involved in the proper growth, development, and function of the central nervous system (CNS). Recent work also suggests that they signal in the context of CNS injury, and that abnormal ciliary signaling may be implicated in neurological diseases.
METHODS: We quantified the distribution of neuronal primary cilia alignment throughout the normal adult mouse brain by immunohistochemical staining for the primary cilia marker adenylyl cyclase III (ACIII) and measuring the angles of primary cilia with respect to global and local coordinate planes. We then introduced two different models of acute brain insult—temporal lobe seizure and cerebral ischemia, and re-examined neuronal primary cilia distribution, as well as ciliary lengths and the proportion of neurons harboring cilia.
RESULTS: Under basal conditions, cortical cilia align themselves radially with respect to the cortical surface, while cilia in the dentate gyrus align themselves radially with respect to the granule cell layer. Cilia of neurons in the striatum and thalamus, by contrast, exhibit a wide distribution of ciliary arrangements. In both cases of acute brain insult, primary cilia alignment was significantly disrupted in a region-specific manner, with areas affected by the insult preferentially disrupted. Further, the two models promoted differential effects on ciliary lengths, while only the ischemia model decreased the proportion of ciliated cells.
CONCLUSIONS: These findings provide evidence for the regional anatomical organization of neuronal primary cilia in the adult brain and suggest that various brain insults may disrupt this organization.

Keywords cerebral cortex, dentate gyrus, temporal lobe seizure, cerebral ischemia

Introduction

The primary cilium is a microtubule-based sensory organelle expressed among most cells of the mammalian body that is critically involved in various signaling pathways (Singla and Reiter, 2006; Berbari et al., 2009; Goetz and Anderson, 2010). Primary ciliary assembly begins at the basal body, a modified centriole that serves as the foundation upon which the ciliary appendage will grow, protruding through the cell membrane. The backbone of the non-motile primary cilium is the axoneme, consisting of cross-linked microtubule doublets in a $9+0$ configuration that provides both tensile strength and a rail upon which intraflagellar transport (IFT) proteins can shuttle to elongate the structure and maintain its integrity (Pedersen and Rosenbaum, 2008; Ishikawa and Marshall, 2011). The importance of this organelle in normal physiology is exemplified by the wide array of ciliopathies that occur when ciliary assembly, anchoring, or signaling is disrupted. Indeed, ciliopathies affecting the neurological, musculoskeletal, endocrine, hepatic, cardiovascular and renal systems have all been well described (Fuchs and Schwark, 2004; Yoder, 2007; Berbari et al., 2008; Quinlan et al., 2008; Ware et al., 2011). In the central nervous system (CNS) in particular, defects in primary cilia that arise during development and throughout life can lead to devastating consequences including hydrocephalus, neurocognitive impairment, and neurodegeneration (Winter et al., 1995; Lee and Gleeson, 2011; Valente et al., 2014).

Received November 18, 2016; accepted January 28, 2017
Correspondence: Qiaojie Xiong
E-mail: Qiaojie.xiong@stonybrook.edu

Others and our own group have previously characterized the development and behavioral relevance of primary cilia in the brain (Breunig et al., 2008; Han et al., 2008; Einstein et al., 2010; Wang et al., 2011; Kumamoto et al., 2012; Rhee et al., 2016). In contrast to the increasingly understood roles of primary cilia in normal development, as well as the well-characterized underlying etiologies of primary ciliopathies, little is known about how neuronal primary cilia respond to cellular and tissue insults. Nevertheless, primary cilia in the CNS appear to be quite sensitive to changes in neurological homeostasis. For instance, signals propagated through neuronal primary cilia aid in mounting a reactive glial response after spinal cord injury, and promote neuronal survival in multiple sclerosis (MS)-induced cortical axonal degeneration, via upregulation of ciliary neurotrophic factor (CNTF) (Winter et al., 1995; Albrecht et al., 2002; Fuchs and Schwark, 2004; Dutta et al., 2007). On the other hand, early neonatal seizure activity can induce structural damage by altering the lengths of primary cilia on cortical neurons (Parker et al., 2016). Although such findings implicate the neuronal primary cilium's involvement in the response or contribution to neurological injury and disease, the global organization of neuronal primary cilia throughout the brain remains unknown, and how this pattern of organization may become grossly or regionally disrupted in the context of brain insults has not been previously studied.

Thus, we first set out to identify neuronal primary cilia patterning throughout the adult brain by examining ciliary positioning in various cortical and subcortical regions. We next examined whether this patterning would become disrupted in two models of acute neurological insult: temporal lobe seizure and cerebral hemispheric ischemia. Our results provide evidence of a gross regional organization of neuronal primary cilia in the brain, and demonstrate a compromise of such organization in the context of two independent models of CNS injury.

Materials and methods

Animals

Eight-week-old female C57BL6 mice (Charles River Laboratories) were used for all experiments. Mice were housed in pairs in standard laboratory cages and maintained on a 12/12 h light/dark cycle with *ad libitum* access to food and water. All surgeries and experimental procedures were approved by the Stony Brook University Animal Use Committee and followed guidelines of the National Institutes of Health.

Immunohistochemistry and quantification

Mice were anesthetized and transcardially perfused with PBS and 4% PFA. Fixed brains were sliced by a sliding microtome, creating 60 μm thick coronal brain sections. Prior to primary antibody incubation, brain sections were blocked with 1% donkey serum in 0.25% Triton-PBS for 1 h. Next, sections were incubated overnight at 4°C with diluted primary antibodies (rabbit anti-adenylyl cyclase III 1:300, goat anti-somatostatin receptor 3 1:300 Santa Cruz Biotechnology, mouse anti-NeuN 1:500, Abcam, goat anti-Iba1, Abcam, mouse anti-Parvalbumin 1:500, Abcam). The next day, brain sections were incubated in diluted secondary antibodies solution (Donkey anti-rabbit CY-3 1:1000, Jackson Laboratories, donkey anti-rabbit AlexaFluoro 647 1:1000, Jackson Laboratories, donkey anti-rabbit Alexa-Fluoro 488 1:1000, Jackson Laboratories, donkey anti-mouse CY-3, 1:1000, Jackson Laboratories, mouse anti-goat Alexa-Fluoro 488 1:1000, Jackson Laboratories, mouse anti-goat CY3 1:1000, Jackson Laboratories) for 4 h at room temperature. Sections were mounted on slides using DAPI-containing mounting media to stain nuclei. All images were acquired on an Olympus FV1000 confocal system.

Primary cilia were identified and related to their neuron of origin by examining 60 μm thick, Z-stacked, 3-dimensional reconstructed images co-stained for ACIII, NeuN, and/or PV using Imaris Scientific 3D/4D Processing & Analysis Software (Bitplane), as we previously described (Rhee et al., 2016). Primary cilia orientation angles were measured in ImageJ by using the perpendicular to the cortical surface as a reference for cortical neurons, the perpendicular to the dorsal/ventral axis for striatal and thalamic neurons, and the perpendicular to the granule cell layer for dentate granule neurons. Primary cilia positions on the neuronal surface were measured identically, with the following exception. The center of the cell soma was used as the vertex for position angles, and the angle extended to the base (proximal attachment point) of the primary cilium. For bent or curved cilia, we measured the proximal angle from the soma to the first point of angulation.

Electroencephalography/electromyography

For EEG/EMG implantation, mice were anesthetized with 1%-2% isoflurane and then placed in a stereotaxic apparatus. Briefly, four stainless screws were inserted into the skull to record the EEG signal. Two EMG wires were inserted under a facial muscle. Both the EEG and EMG channel were connected to a headmount (#8402, Pinnacle Technology) and then secured with dental cement. Mice were allowed to recover from surgery on a 37°C heating pad for two hours and were administered buprenorphine HCl (0.05 mg/kg, i.p.) for immediate post-surgery analgesia. Mice were given 2 weeks for recovery. During recording, freely moving animals were placed in a soundproofed box with a video recording system, with food and water provided *ad libitum*. EEG/EMG signals were amplified (X100), filtered (0.5-25 Hz for EEG, 10-100 Hz for EMG), digitalized and then recorded with Sirenia Acquisition software (Pinnacle Technology). After 30 min of baseline recording, mice were injected with scopolamine (1 mg/kg dissolved in 0.9% NaCl, i.p.), followed by pilocarpine

15 min later (300 mg/kg dissolved in 0.9% NaCl, i.p.) to induce seizure. EEG/EMG signals and video were continuously monitored, and both EEG and EMG responses were compared before and after seizure. A second group of animals received identical treatment but were administered 0.9% NaCl instead of pilocarpine to serve as a control group. Mice were sacrificed 4.5 h after pilocarpine or saline treatment. The reasons for choosing this early time point were twofold: 1) We were interested in the acute phase of temporal lobe seizure, during which time mitochondrial respiration becomes compromised, but before the onset of diffuse metabolic derangements leading to decreased neuronal respiration and reserve capacity (beginning after 12 h and lasting ~6 weeks) (Rowley et al., 2015); 2) We were concerned about the variable post-ictal survival rate we observed (data not shown) and as such, the potential for variation in severity of neurological sequalae that could result from more intermediate to chronic time points.

Internal carotid artery occlusion

We performed internal carotid artery occlusion similar to what has been previously described (Yin et al., 2010). Briefly, mice were anesthetized with ketamine/xylazine cocktail (200 mg/kg i.p.). A 2 cm vertical midline incision was made inferior to the chin and subcutaneous glandular tissue was retracted with sterile saline-soaked Q-tips. Blunt dissection was used to access the carotid sheath, and a 4-0 non-absorbable sterile silk suture tie was used to ligate the external carotid artery at its origin. The internal carotid artery was then identified and ligated with a 4-0 non-absorbable sterile silk suture tie. The incision was closed with non-absorbable sterile nylon suture. A sham surgery control group received identical treatment without suture placement. Mice were allowed to recover from surgery on a 37°C heating pad for two hours, were administered buprenorphine HCl (0.05 mg/kg, i.p.) for immediate post-surgery analgesia, and were continuously monitored via video recording. Mice were sacrificed 12 h after surgery, at which time prolonged ischemia is sufficient to induce acute neuronal changes (e.g. dendritic vacuolation and cellular scalloping, shrinkage, and/or swelling) but before the onset of more severe and widespread cellular changes (e.g., cytoplasmic eosinophilia, karyolysis, necrosis) (Garcia et al., 1993).

Analysis and statistics

Data were analyzed with two-sample Kolmogorov–Smirnov non-parametric tests of equality and the binomial test. Alpha values of less than 0.05 were considered the cut-off for statistical significance for all tests. Data are represented as mean ± standard error of the mean (SEM) unless otherwise specified. All statistics presented in figures are represented as $P < 0.05$ or $P < 0.01$. P values are greater than 0.05 unless otherwise indicated.

Results

Cortical neurons displayed a radial alignment of primary cilia

To determine whether cortical neuronal primary cilia exhibit a pattern of alignment in the normal adult brain, we first measured primary cilia angles and cellular positioning. We selected four cortical regions around the circumference of the cortex (primary visual cortex, V1; lateral aspect of secondary visual cortex, V2L; primary auditory cortex, A1; and entorhinal cortex, Ent), in order to assess for patterns of ciliary alignment. We measured the angle of the primary cilium on the polar coordinate axis with respect to a perpendicular drawn to the cortical surface, as well as the relative position of the primary cilium's base with respect to the cell body (i.e. the "clock face" position) (Fig. 1A). Measurements taken from the left hemisphere were reflected over the *y*-axis before analysis, while those taken from the right hemisphere were analyzed directly, in order to ensure that angles measured from both hemispheres were compared to each other on the same global coordinate plane. We began by confirming the identity of neuronal primary cilia by co-immunostaining for two neuronal ciliary proteins, adenylyl cyclase III (ACIII) and somatostatin receptor 3 (SSTR3) (Handel et al., 1999; Bishop et al., 2007), and observed robust co-localization, as expected (Fig. 1B).

We observed a radial pattern of primary cilia angle and position distributions when we co-immunostained for ACIII and the neuronal marker NeuN (Wolf et al., 1996), from V1 circumferentially to Ent (Fig. 1C-F; Fig. 2A-D). To determine whether the radial alignment is a general property of all cortical primary cilia, or is layer-specific, we further parsed these distributions of angles and positions by performing a subgroup analysis on the neuronal primary cilia of the different cortical layers (L I, L II/III, L IV, L V, L VI). We observed a clear trend of radial ciliary angles and positions in layers II-VI in all four regions examined (Figs. S1, S2). However, L I displayed a wide distribution of angles (standard deviation (SD) of angles, V1: 95.4°, V2L: 35.4°, A1: 94.4°, Ent: 72.7°; SD of positions, V1: 34.7°, V2L: 142.8°, A1: 56.7°, Ent: 98.0°) (Figs. S1, S2).

We noted that the radial alignment of primary cilia largely corresponded to the orientation of the apical dendrite of the major population of cortical neurons, i.e. the pyramidal neurons (Spruston, 2008), although we noted variation in the distributions among the regions and cortical layers. We hypothesized that some of the variation of ciliary angles and positions would be at least partially accounted for by cilia of cortical GABAergic interneurons, which lack a dominant apical dendrite (Benes and Berretta, 2001). As expected, we found a wide variation in ciliary angles and positions among the Parvalbumin (PV)-positive group of interneurons in all four cortical regions examined (SD of angles, V1: 131.6°, V2L: 105.5°, A1: 72.5°, Ent: 113.8°; SD of positions, V1:

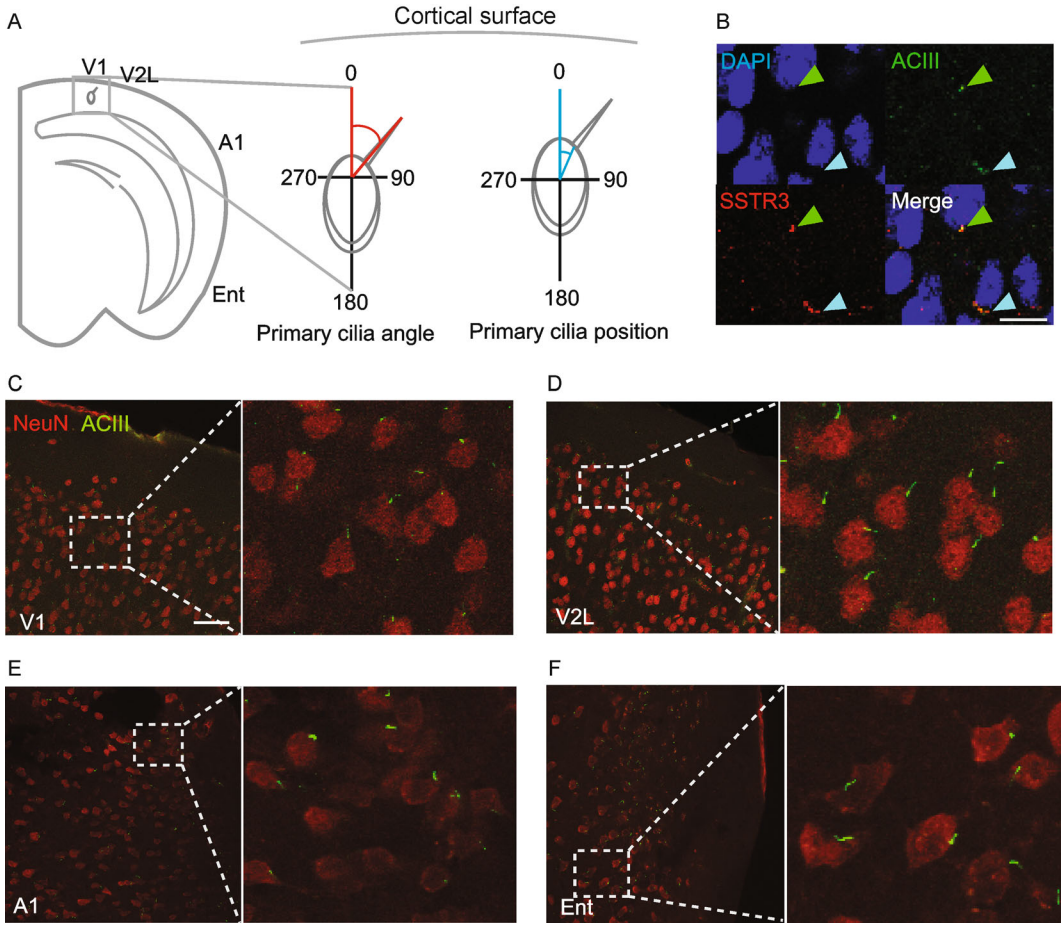

Figure 1 Neuronal primary cilia are radially aligned throughout the cortex. (A) Shown is a schematic of the primary cilia angle and position measurements (°). (B) Shown is a representative image of a cell stained for adenylyl cyclase III and somatostatin receptor 3 (SSTR3). The scale bar is 30 μm. (C) Shown is a representative image of neurons and their primary cilia in area V1. The scale bar is 50 μm. (D) Shown is a representative image of neurons and their primary cilia in area V2L. (E) Shown is a representative image of neurons and their primary cilia in area A1. (F) Shown is a representative image of neurons and their primary cilia in area Ent.

117.6°, V2L: 130.4°, A1: 97.1°, Ent: 122.6°) (Fig. S3). Together, these results show that a majority of cortical neuronal primary cilia align radially with respect to the cortical surface, while interspersed GABAergic interneurons exhibit a wide distribution of ciliary organization.

Striatal and thalamic neurons exhibited a wide distribution of ciliary alignment, while those of dentate granule neurons exhibited a radial alignment with respect to the granule cell layer

Given the cortical organization of primary cilia we observed, we next sought to determine whether any such pattern would emerge among subcortical neuronal populations that connect with the superficial cortex. We thus examined two such regions, one that projects to neocortex: the anterior nucleus of the thalamus (Thal), and one that receives neocortical projections: the dorsal striatum (DStr) (Irle and Markowitsch, 1982; Pan et al., 2010). We analyzed ciliary orientations with respect to the vertical perpendicular, and ciliary positions with respect to the cell body for DStr and Thal (Fig. 3A). We observed a wide variation in ciliary angles and positions in DStr (SD of angles: 116.3°; SD of positions: 116.8°) as well as in thalamus (SD of angles: 101.0°; SD of positions: 95.5°) (Fig. 3B,C; Fig. 4A-B).

We finally examined a unique deep cortical structure that receives projections from the more superficial entorhinal cortex: the dentate gyrus (DG) of the hippocampal formation. Unlike the thalamus and striatum, the DG contains its own internal plane of alignment: the subgranular zone (SGZ). Mature DGCs align radially with respect to the SGZ as they mature and integrate into the hippocampal circuit (Zhao et al., 2006). We therefore wondered whether primary cilia of dentate granule cells (DGCs) would align themselves with respect to this local axis as do their cells of origin. We measured ciliary orientation with respect to the SGZ as indicated in Fig. 3D, and measured ciliary position as described above. We observed a radial distribution of ciliary

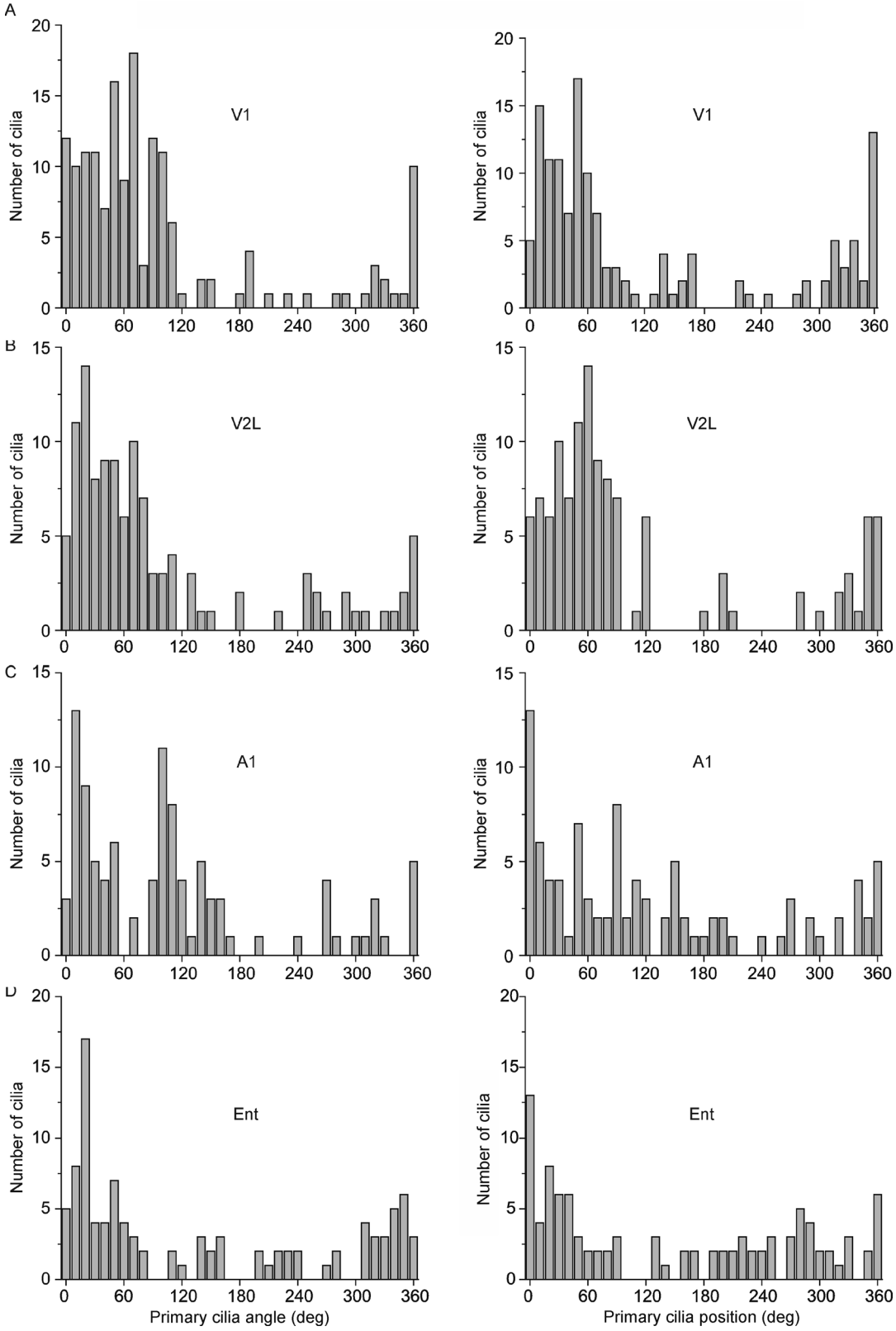

Figure 2 Neuronal primary cilia alignment in the cortex. (A) Shown are the distribution of angles (°) of primary cilia with respect to the cortical surface (left) and with respect to the soma (right) in area V1. (B) Shown are the distribution of angles (°) of primary cilia with respect to the cortical surface (left) and with respect to the soma (right) in area V2L. (C) Shown are the distribution of angles (°) of primary cilia with respect to the cortical surface (left) and with respect to the soma (right) in area A1. (D) Shown are the distribution of angles (°) of primary cilia with respect to the cortical surface (left) and with respect to the soma (right) in area Ent. Angle: $N = 159$ cells (V1), 116 cells (V2L), 102 cells (A1), 101 cells (Ent); Position: $N = 141$ cells (V1), 118 cells (V2L), 102 cells (A1), 101 cells (Ent) from 4 animals.

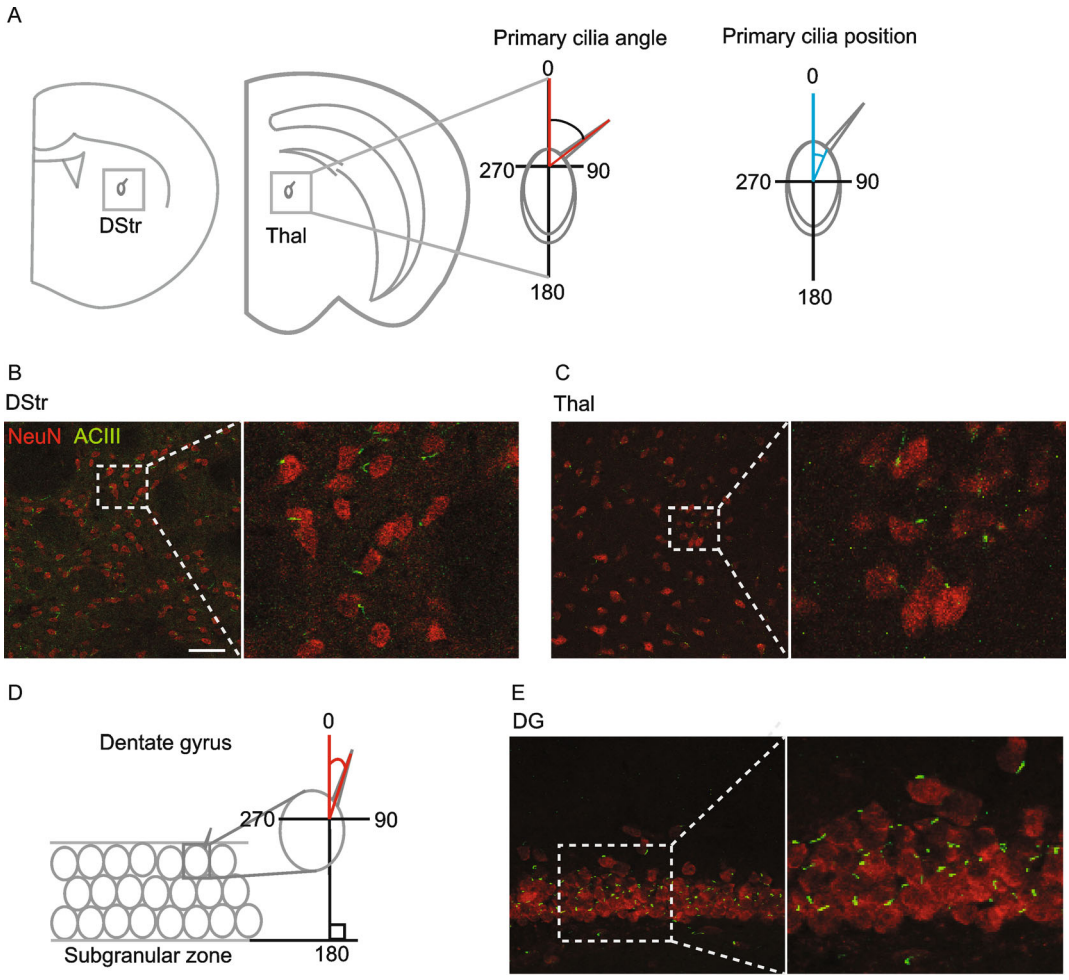

Figure 3 Neuronal primary cilia alignment in dorsal striatum, thalamus, and dentate gyrus. (A) Shown is a schematic of the primary cilia angle and position measurements (°) in dorsal striatum (DStr) and thalamus (Thal). (B) Shown is a representative image of neurons and their primary cilia in the dorsal striatum. The scale bar is 50 μm. (C) Shown is a representative image of neurons and their primary cilia in the anterior nucleus of the thalamus. (D) Shown is a schematic of the primary cilia angle measurement in the dentate gyrus (DG) with respect to the subgranular zone (SGZ). (E) Shown is a representative image of neurons and their primary cilia in the DG. $N = 4$ animals.

angles and positions, clustering between 0 and 90° (53.1± 23.5°) and 270-360° (312.8±28.7°) for orientation, and clustering between 0 and 90° (35.8±20.7°) and 270-360° (324.3±20.2°) for position (Fig. 3D, E; Fig. 4C). Thus, primary cilia of DGCs tended to align perpendicular to the GCL. Taken together, these findings demonstrate that neuronal primary cilia in DStr and Thal exhibit a wide variation in alignment with respect to the global axis, while those in DG align radially with respect to the GCL.

Primary cilia organization in the cortex was disrupted by pilocarpine-induced seizure

To determine whether primary cilia organization would be disrupted in a pathological context, we examined cortical primary cilia after pilocarpine-induced seizure, commonly used in rodent models of temporal lobe epilepsy, with seizure foci originating in the entorhinal cortex and hippocampus (Curia et al., 2008). We followed a seizure induction protocol as previously described (Marchi et al., 2007). Briefly, we assigned mice that had been implanted with a cortical EEG headmount and intramuscular EMG to receive intraperitoneal injections of scopolamine (1 mg/kg i.p.) followed by either pilocarpine (300 mg/kg i.p.; $N = 5$ animals) or saline as control ($N = 5$ animals), and recorded EEG and EMG activity at baseline and after injection. As illustrated in Fig. 5A, we observed robust seizure activity minutes after pilocarpine induction. Comparing the EEG power spectra from saline- and pilocarpine-injected mice, we observed increased peak power in the delta and theta range (Fig. 5A), as expected (Pessoa et al., 2016). Four and a half hours after pilocarpine or saline administration, we sacrificed mice to examine neuronal primary cilia.

We observed that pilocarpine induced a significant shift in the distribution of neuronal primary cilia positioning in all four cortical regions examined (Fig. 5B-E). In dorsal cortical

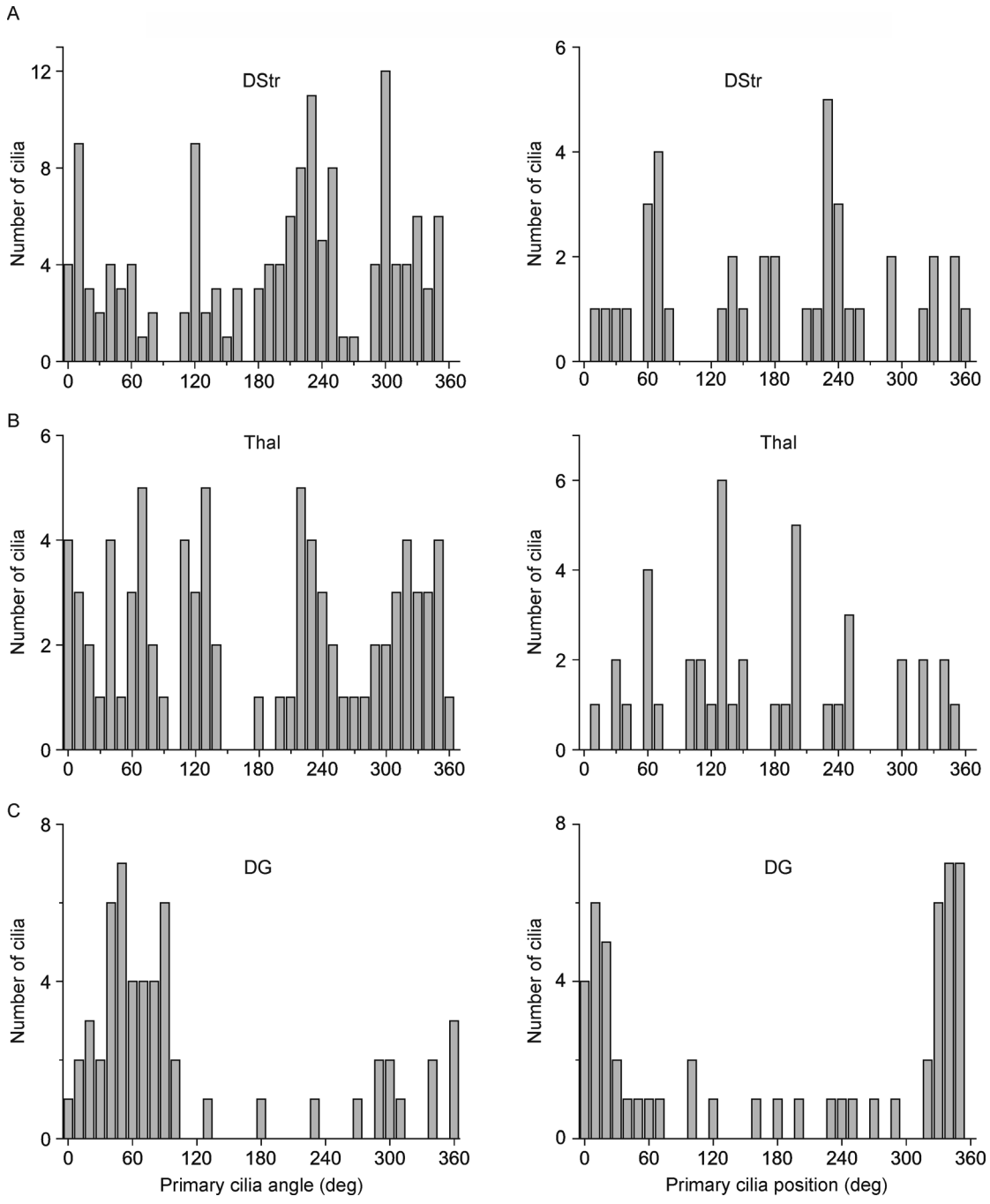

Figure 4 Distribution of neuronal primary cilia angles and positions in dorsal striatum, thalamus, and dentate gyrus. (A) Shown are the distribution of angles (left) and positions (right) of primary cilia with respect to the cortical surface (°) in DStr. (B) Shown are the distribution of angles (left) and positions (right) of primary cilia with respect to the cortical surface (°) in Thal. (C) Shown are the distribution of angles (left) and positions (right) of primary cilia with respect to the cortical surface (°) in DG. Angle: $N = 142$ cells (DStr), 82 cells (Thal), 55 cells (DG); Position: $N = 40$ cells (DStr), 43 cells (Thal), 55 cells (DG) from 4 animals.

areas, pilocarpine induced a counterclockwise shift in primary cilia positioning with respect to the radial axis, while in the ventral cortex, pilocarpine induce a clockwise shift in primary cilia positioning. We further observed that pilocarpine induced a significant shift in the distribution of primary cilia orientation in A1 and Ent, but did not significantly affect those of V1 or V2L (Fig. 5B-E).

Primary cilia organization in dorsal striatum and dentate gyrus was disrupted by pilocarpine-induced seizure

We next wondered whether pilocarpine-induced seizure would alter the organization of neuronal primary cilia in deeper brain structures, especially the hippocampus in which pilocarpine-induced seizures originate. We again measured

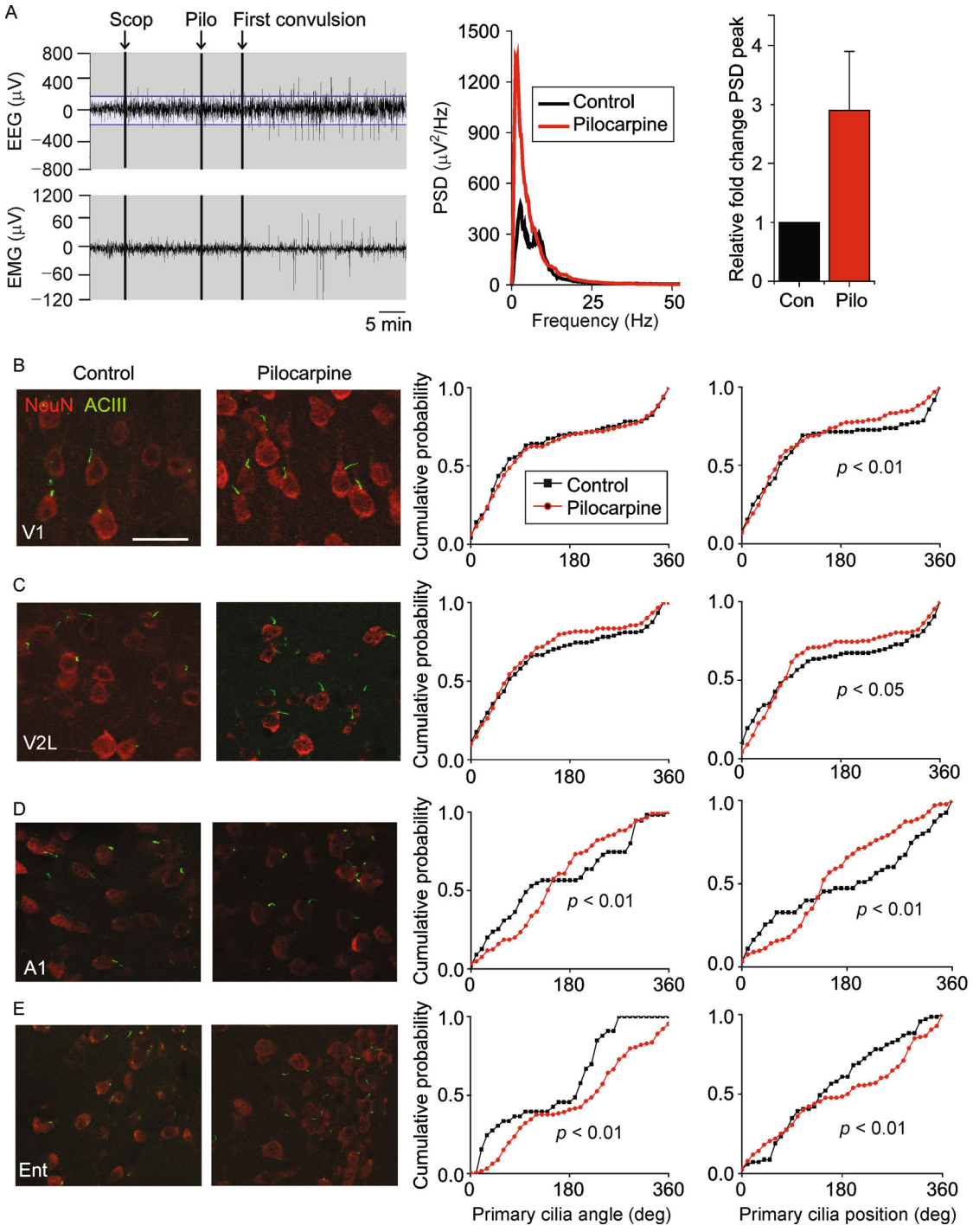

Figure 5 Pilocarpine-induced seizure disrupted primary cilia alignment in cortical neurons. (A) On the left are representative EEG and EMG traces taken from an animal injected with scopolamine (Scop) followed by pilocarpine (Pilo). The corresponding power spectrum density graph is shown in the center. On the right is a graph of the peak power for all animals in the Contrl (Con) and Pilo groups. (B) Shown on the left are representative images of neurons and their primary cilia in area V1 in the control and pilocarpine conditions. On the right are distribution plots of primary cilia angle and position (°). The scale bar is 30 μm. (C) Shown on the left are representative images of neurons and their primary cilia in area V2L in the control and pilocarpine conditions. On the right are distribution plots of primary cilia angle and position (°). (D) Shown on the left are representative images of neurons and their primary cilia in area A1 in the control and pilocarpine conditions. On the right are distribution plots of primary cilia angle and position (°). (E) Shown on the left are representative images of neurons and their primary cilia in area Ent in the control and pilocarpine conditions. On the right are distribution plots of primary cilia angle and position (°). Two-sample Kolmogorov–Smirnov tests: V1 angle (synonymous with orientation): $P > 0.05$, V1 position: $P = 0.001$, $N = 84$ cells (control), 186 cells (pilocarpine); V2L angle $P > 0.05$, V2L position: $P = 0.049$, $N = 105$ cells (control), 169 cells (pilocarpine); A1 angle: $P = 0.001$, A1 position: $P < 0.001$, E1: $P < 0.001$, $N = 55$ cells (control), 134 cells (pilocarpine); Ent angle: $P < 0.001$, Ent position: $P < 0.001$, $N = 68$ (control), 128 (pilocarpine) cells from 5 animals per group.

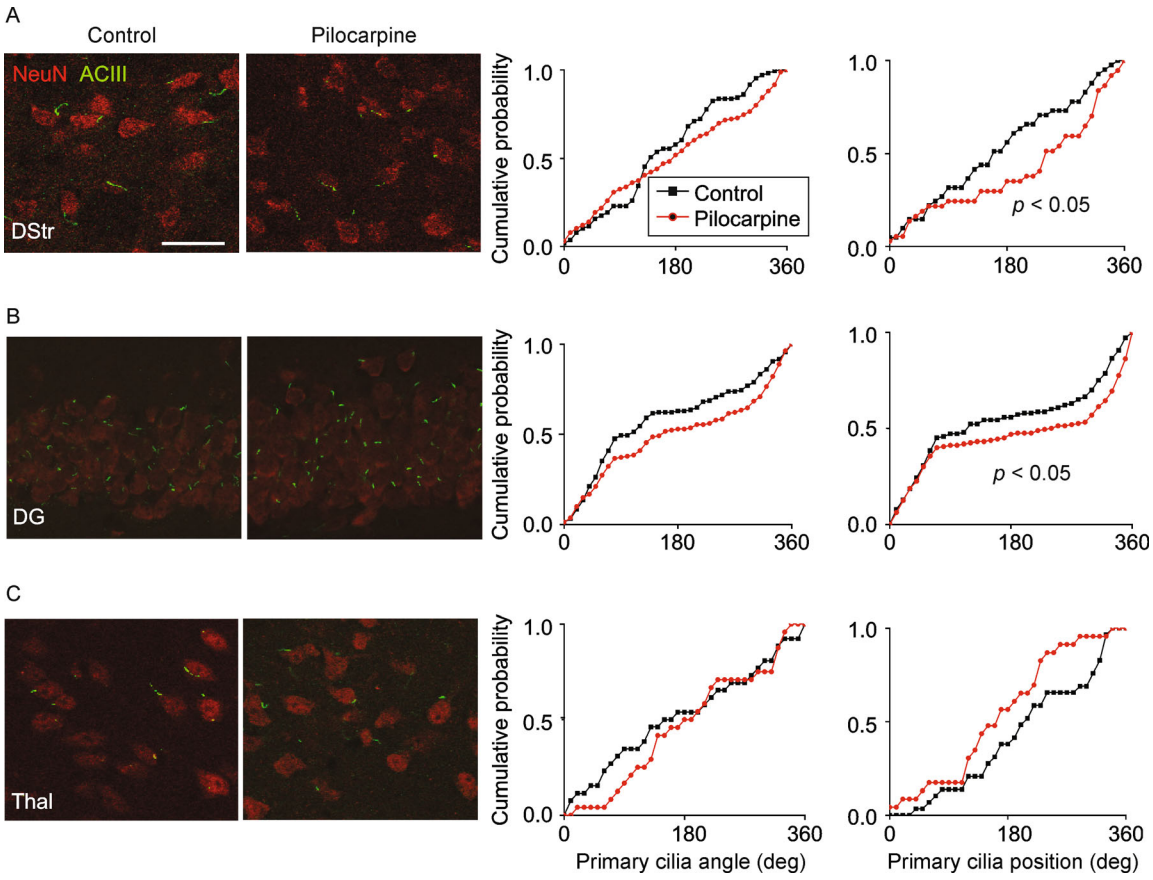

Figure 6 Pilocarpine-induced seizure disrupted primary cilia alignment in hippocampal and striatal neurons. (A) Shown on the left are representative images of neurons and their primary cilia in DStr in the control and pilocarpine conditions. On the right are distribution plots of primary cilia angle and position (°). The scale bar is 30 µm. (B) Shown on the left are representative images of neurons and their primary cilia in DG in the control and pilocarpine conditions. On the right are distribution plots of primary cilia angle and position (°). (C) Shown on the left are representative images of neurons and their primary cilia in Thal in the control and pilocarpine conditions. On the right are distribution plots of primary cilia angle and position (°). Two-sample Kolmogorov–Smirnov tests, DStr position: $P = 0.014$, $N =$ 195 cells (control), 87 cells (pilocarpine), DG position: $P = 0.023$ $N = 140$ cells (control), 160 cells (pilocarpine) from 5 animals per group.

ciliary orientation and positions in DStr, Thal, and DG. We measured angles with respect to the global axis in the cases of DStr and Thal, and with respect to the GCL in the case of the DG, as above. We observed a significant shift in the distribution of primary cilia positions in DStr and DG (Fig. 6A,B). No significant shifts in cilia angle or position were noted in Thal (Fig. 6C).

Together, these data show that pilocarpine-induced seizure alters the radial positioning of primary cilia on cortical, dentate granule, and striatal neurons.

Primary cilia organization was regionally disrupted by ischemic brain injury

We next examined primary cilia distributions in the context of an ischemic brain injury. We induced cerebral ischemia by occluding the left internal carotid artery, as previously described (Yin et al., 2010). Mice were randomly assigned to receive either carotid artery occlusion ($N = 3$ animals) or sham surgery ($N = 3$ animals) and sacrificed 12 h later (Fig. 7A). We verified the sufficiency of cerebral ischemia induction by monitoring animal behavior post-surgery, noting contralateral hemiparesis in occluded mice but not in sham controls, as expected (data not shown). We further immunostained brain sections for the microglia/macrophage marker Iba1, to assess for microglial infiltration of the site of ischemia, as previously described (Inose et al., 2015). We noted marked microglial infiltration on the ipsilateral side in occluded mice but not on the contralateral side, or in sham surgery controls, as expected (Fig. 7A). Twelve hours after occlusion of the internal carotid artery, we observed significant shifts in primary cilia orientations in A1 and Ent, and significant disruptions in primary cilia positioning in A1, V1 and V2L (Fig. 7B-E). We then analyzed the primary cilia in DG, DStr, and Thal, and found a significant effect of carotid artery occlusion on ciliary positioning in the DG, but observed no significant effects of on orientation or positioning in DStr or Thal (Fig. 8A-C).

Together, these results suggest that acute ischemic brain injury induces disruptions in primary cilia alignment. Moreover, the regional effects of ischemia on primary cilia we observed are generally consistent with the blood supply

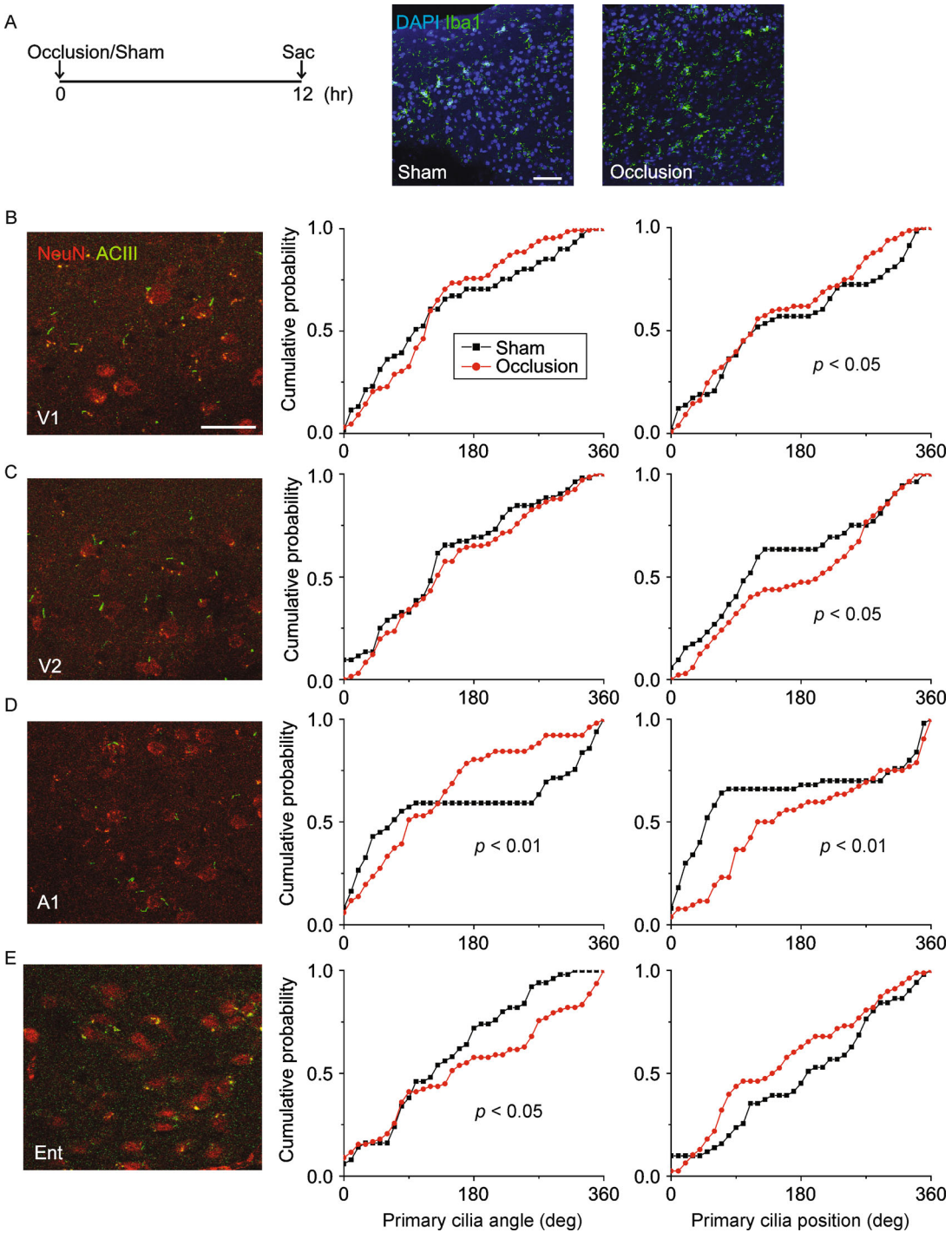

Figure 7 Internal carotid artery occlusion disrupted primary cilia alignment in cortical neurons. (A) Shown on the left is the experimental procedure timeline. On the right are representative images of Iba1-stained sections taken from the infarct region from an animal in the occlusion condition side-by-side with a sham-operated control. The scale bar is 50 μm. (B) Shown on the left are representative images of neurons and their primary cilia in area V1 in the occlusion condition. On the right are distribution plots of primary cilia angle and position (°). (C) Shown on the left are representative images of neurons and their primary cilia in area V2L in the occlusion condition. On the right are distribution plots of primary cilia angle and position (°). (D) Shown on the left are representative images of neurons and their primary cilia in area A1 in the occlusion condition. On the right are distribution plots of primary cilia angle and position (°). (E) Shown on the left are representative images of neurons and their primary cilia in area A1 in the occlusion condition. On the right are distribution plots of primary cilia angle and position (°). Two-sample Kolmogorov–Smirnov tests: V1 position: $P = 0.039$, $N = 59$ cells (sham), 99 cells (occlusion); V2L position: $P = 0.017$, $N = 53$ cells (sham), 132 cells (occlusion); A1 angle: $P = 0.004$, A1 position: $P < 0.001$, $N = 50$ cells (sham), 53 cells (occlusion); Ent angle: $P = 0.042$, $N = 51$ cells (sham), 83 cells (occlusion) from 3 animals per group.

occluded in our model, with the most severe and significant effects noted in areas supplied by the occluded middle cerebral artery, including the temporal and parietal lobes, although we still detected subtle but significant changes in other regions (Coyle, 1976; Dorr et al., 2007).

Seizure and ischemia induced changes in primary cilia length, while only ischemia affected the number of ciliated neurons

Given that structural integrity of neuronal primary cilia can become compromised in ways other than their orientation (e.g. their length) in the context of neurological insult (Parker et al., 2016), we finally set out to determine whether pilocarpine-induced seizure or carotid artery occlusion-induced ischemia would acutely affect the number of ciliated neurons or the lengths of neuronal primary cilia.

To identify any potential disruption in ciliary lengths and the number of ciliated versus non-ciliated neurons in the pilocarpine-induced seizure model, we examined one cortical region (Ent) and its synaptically targeted subcortical region (DG). We observed significantly greater ciliary lengths in Ent neurons of pilocarpine-injected mice as compared to control mice (Fig. 9A). By contrast, we observed no significant

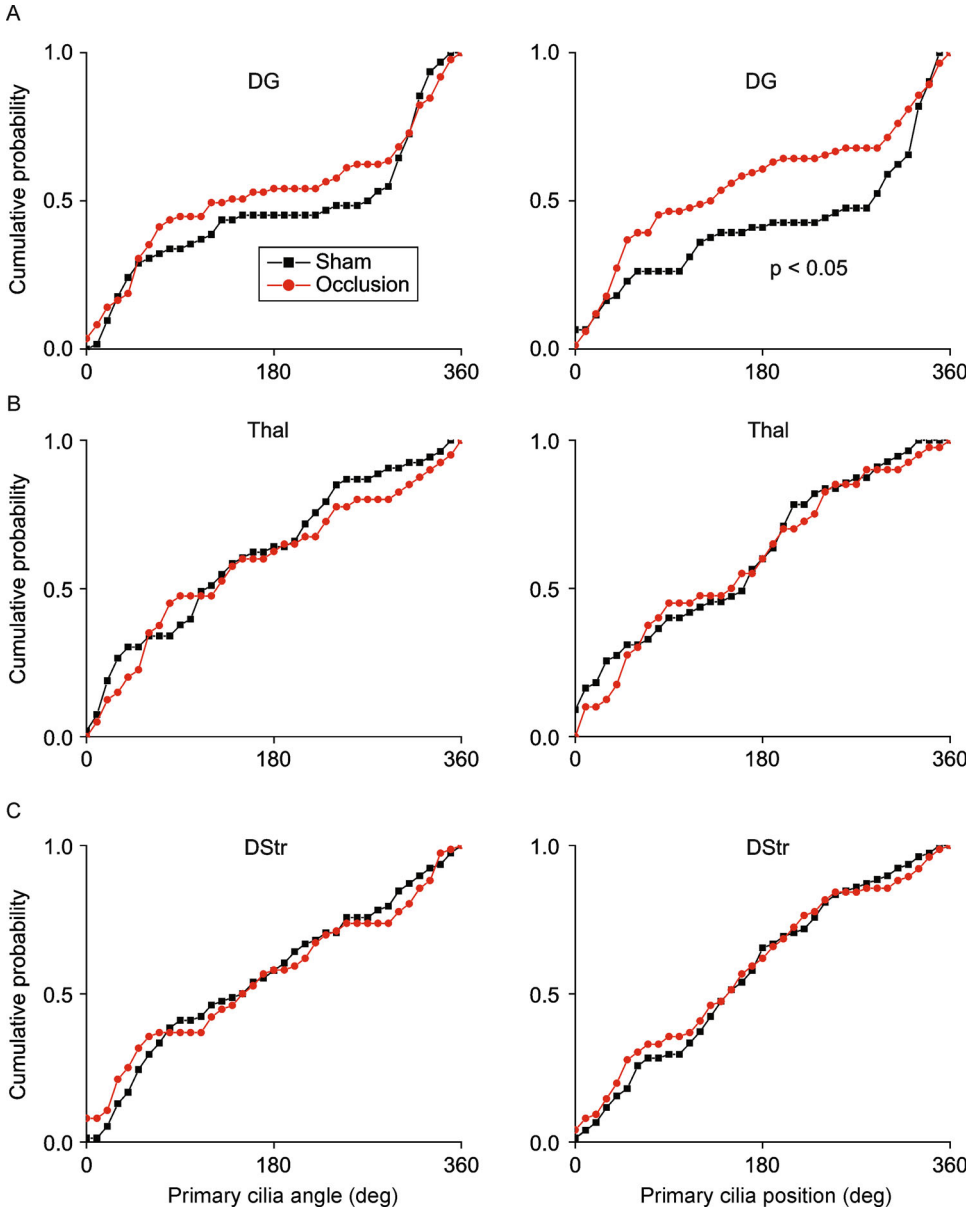

Figure 8 Internal carotid artery occlusion affected primary cilia alignment in the dentate gyrus but not in striatum or thalamus. (A) Shown are distribution plots of primary cilia angle and position (°) in DG. (B) Shown are distribution plots of primary cilia angle and position (°) in Thal. (C) Shown are distribution plots of primary cilia angle and position (°) in DStr. Two-sample Kolmogorov–Smirnov tests: DG angle: $P > 0.05$, DG position: $P = 0.011$, $N = 61$ cells (sham), 85 cells (occlusion); Thal angle: $P > 0.05$, Thal position: $P > 0.05$, $N = 55$ cells (sham), 40 cells (occlusion); DStr orientation: $P > 0.05$, DStr orientation: $P > 0.05$, $N = 78$ cells (sham), 76 cells (occlusion).

difference in ciliary lengths in the DG (Fig. 9A). The proportion of cells that were ciliated was comparable between groups in both regions examined (Fig. 9B).

We next analyzed ciliary lengths and the number of ciliated versus non-ciliated cells in the carotid artery occlusion model of ischemia. We observed significantly shorter cilia in both Ent and DG, as compared to sham surgery controls (Fig. 9C). Strikingly, when we analyzed the proportion of ciliated neurons, we observed dramatic reductions in both Ent and DG in occluded animals as compared to sham controls (Fig. 9D).

Taken together, these results suggest that pilocarpine-induced seizure has regionally variable effects on neuronal primary cilia lengths, without affecting the total number of ciliated cells. By contrast, the carotid artery occlusion ischemia model induced consistent shortening of cilia lengths and also decreased the number of ciliated cells across brain regions.

Discussion

In this study, we systematically mapped the organization of neuronal primary cilia throughout the adult mouse brain. We made the interesting discovery that neurons in neocortex display their primary cilia radially, in line with the orientation

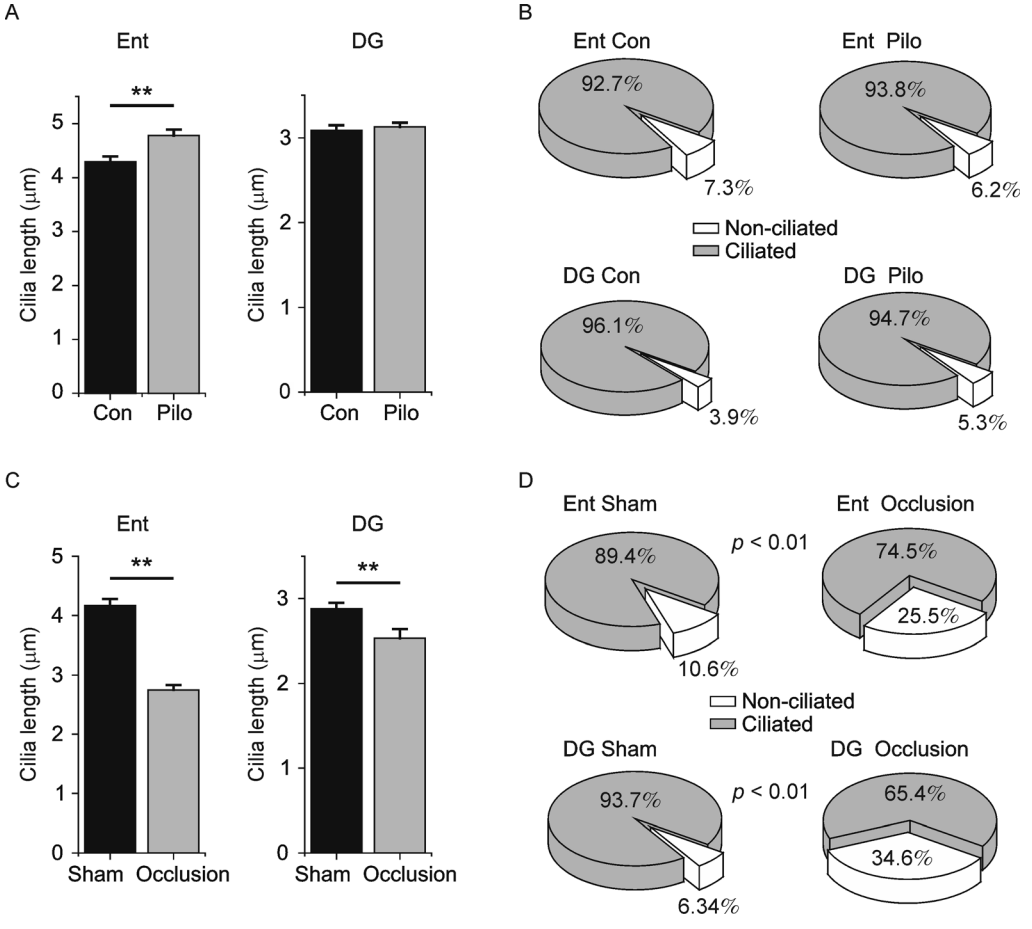

Figure 9 Primary cilia length and number in seizure and ischemia. (A) Shown are plots of cilia lengths measured in entorhinal cortex (Ent) and dentate gyrus (DG) in mice injected with pilocarpine (Pilo) or saline (Con). Ent con: 4.27±0.11 μm, Ent pilo 4.54±0.11 μm, Kolmogorov–Smirnov test $P < 0.001$, $N = 105$, 199 cells, respectively; DG con: 3.09±0.06 μm, pilo: 3.13±0.05 μm, Kolmogorov–Smirnov test $P > 0.05$, $N = 250$ cells/group from 3 animals/group. (B) Shown are pie charts displaying the proportion of neurons containing (gray wedge) or lacking (white wedge) primary cilia in Ent and DG of Pilo and Con animals. Ent con: 190/205 cells ciliated, Ent Pilo: 212/226 cells ciliated, binomial test $P > 0.05$; DG Con: 355/370 cells ciliated, DG Pilo: 319/337 cells ciliated, binomial test $P > 0.05$. (C) Shown are plots of cilia lengths measured in entorhinal cortex (Ent) and dentate gyrus (DG) in mice that received carotid artery occlusion (Occlusion) or sham surgery (Sham). Ent sham: 4.17±0.11 um, Ent occlusion: 2.75±0.08 um, Kolmogorov–Smirnov test $P < 0.001$, $N = 150$, 161 cells, respectively; DG sham: 2.88±0.07 um, DG occlusion: 2.54±0.11 um, Kolmogorov–Smirnov test $P = 0.001$, $N = 100$, 56 cells, respectively. (D) Shown are pie charts displaying the proportion of neurons containing (gray wedge) or lacking (white wedge) primary cilia in Ent and DG of Occlusion and Sham animals. (Ent sham: 186/208 cells ciliated, Ent occlusion: 117/157 cells ciliated, binomial test $P < 0.001$; DG sham: 399/426 cells ciliated, DG occlusion: 219/335 cells ciliated, binomial test $P < 0.001$. ** represents $P < 0.01$.

of their cells of origin. Likewise, dentate granule neurons in the DG display their primary cilia radially with respect to the GCL, as the neurons themselves are poised. This radial alignment likely corresponds to the orientation of the apical dendrite (Kumamoto et al., 2012), as GABAergic interneurons lacking a dominant apical dendrite exhibited no clear pattern of primary cilia alignment (Fig. S3). We then investigated whether this intrinsic ciliary order would become acutely disrupted in pathological settings. Indeed, we observed significant shifts in the distribution of primary cilia angles and positioning on the cell in a temporal lobe seizure model (Figs. 5-6) and an ischemic stroke model (Figs. 7-8). Importantly, areas affected by these insults were generally more severely affected than those that were relatively spared, with respect to preservation of cilia orientation.

Neuronal primary cilia play important functions in normal cerebral development and homeostasis. Primary cilia regulate the proliferation of neural progenitors and dictate neural patterning and midbrain-hindbrain boundary determination during embryogenesis (Han and Alvarez-Buylla, 2010). In the healthy adult brain, primary cilia also promote the division and maturation of hippocampal neurons (Breunig et al., 2008; Kumamoto et al., 2012). As sensory structures, neuronal primary cilia signal through G protein-coupled receptors (GPCRs), adenylyl cyclase, and calcium channels, allowing them to act as efficient chemosensors in the CNS (Fuchs and Schwark, 2004; DeCaen et al., 2013). This property makes them particularly well suited to rapidly detect local changes in the brain's microenvironment that may be the first signals of acute CNS insult, such as synchronized epileptiform discharge or hypoxia. Indeed, previous work has demonstrated that primary cilia are involved in axonal repair and glial scar formation after injury (Winter et al., 1995; Albrecht et al., 2002; Dutta et al., 2007).

On the other hand, loss of the integrity of primary cilia during neuronal injury may exacerbate the offense and impede functional recovery. A recent study found that primary cilia development was sensitive to PTZ or KA-induced seizures in the early postnatal period (Parker et al., 2016). In that investigation, the lengths of primary cilia were disrupted upon seizure induction, with neocortical and hippocampal cilia lengthening, shortening, or exhibiting no change, depending on the specific brain region, the developmental age of the animal, and the seizure induction protocol. Interestingly, a single perinatal seizure was sufficient to induce long-lasting effects on neuronal primary cilia length, as measured up to 42 days post-natally. In the present study, we focused on the pre-existing neuronal cilia of the adult brain, rather than newly-sprouting cilia. We observed shifts in the distribution of cilia angles and positioning on neurons of pilocarpine-treated animals in all cortical regions examined, as well as in the dorsal striatum and dentate gyrus, with thalamic sparing (Figs. 5-6). We also found significant cilia lengthening in one cortical region examined, although there was no change in this parameter in the dentate gyrus (Fig. 9). The more severe effects we observed in the temporal lobe/limbic structure as compared to other structures is consistent with the focus of temporal lobe epileptiform discharge (Curia et al., 2008).

Furthermore, in our cerebral ischemia model, we observed significant effects on cilia orientation in neocortical regions as well as in the dentate gyrus (Figs. 7-8). We also identified changes in cilia lengths and the percentage of ciliated cells in this model (Fig. 9). These disruptions likewise generally correlated with areas supplied by branches of the middle cerebral artery (Dorr et al., 2007), which was occluded in our model.

The effects on cilia orientation and length we observed may represent structural damage induced to the neuronal cytoskeleton under metabolic stress. For example, hypoxic conditions can induce changes in the neuronal cytoskeleton by interfering with actin assembly and loss of microtubule-associated proteins (Ota et al., 1997; Khan et al., 2008). The primary cilium emerges from the basal body, derived from the mother centriole, whose localization/polarization is highly dependent upon the microtubule- and microfilament-based infrastructure of the cytoskeleton (Buendia et al., 1990). Thus, any damage to this cellular scaffolding system could potentially result in a bending or distortion of the primary cilium, as we discovered in our two models of acute brain injury.

Alternatively, or in addition, such changes in primary cilia could serve as an initial signal to surrounding neurons and glial cells that damage has occurred. For example, Double-cortin domain containing 2 (DCDC2) is a cilia- and microtubule-localizing protein that interfaces between the primary cilium and the cytoskeleton to regulate Sonic hedgehog (Shh) and Wnt signaling (Massinen et al., 2011). Importantly, the Wnt/beta-catenin pathway has been shown to be induced by both seizure activity and hypoxia (Busceti et al., 2007; Theilhaber et al., 2013). Given the vital role that beta-catenin plays in the maintenance of neuronal structural integrity as well as synaptic plasticity (Maguschak and Ressler, 2012; Theilhaber et al., 2013), it is plausible that this pathway could be disrupted when primary cilia become compromised, as in the two pathological contexts we examined. Still, it will be important to pinpoint the mechanisms by which neurological insult results in acute changes in cilia orientation and length, and to identify the functional consequences thereof.

While signaling downstream of structurally-compromised neuronal primary cilia remains to be determined, pathways may have been triggered to promote aberrant neurite outgrowth or progenitor cell proliferation, which are known to occur in seizure and ischemia models (Yagita et al., 2001; Huang et al., 2002; Madsen et al., 2003; Parent et al., 2006; Sierra et al., 2015). With regard to cerebral ischemia, upregulated cytokine signaling (e.g. via tumor necrosis factor (TNF)) and microglia recruitment are among the hallmarks of

the acute response (Bruce et al., 1996). The potential role of primary cilia in this setting remains uncertain, and should be the focus of future investigation.

In summary, we have shown that neuronal primary cilia display a region-specific distribution of alignment, and that this patterning becomes acutely disrupted during brain injury. Whether preventing neuronal primary cilia from modifying their alignment or length in the context of CNS injury would alleviate or exacerbate cellular damage and functional recovery will be important questions to address in future work.

Acknowledgements

This work was supported by 1R21AG046875 and R01NS089770 to S.G., 1F30MH110103 to G.W.K., and departmental internal funding to Q.X., and the Simons Summer Research Program (SSRP) to Tracy Lang.

Compliance with ethics guidelines

Gregory W. Kirschen, Hanxiao Liu, Tracy Lang, Xuelin Liang, Shaoyu Ge, and Qiaojie Xiong declare that they have no conflicts of interest. All institutional and national guidelines for the care and use of laboratory animals were followed.

References

Albrecht P J, Dahl J P, Stoltzfus O K, Levenson R, Levison S W (2002). Ciliary neurotrophic factor activates spinal cord astrocytes, stimulating their production and release of fibroblast growth factor-2, to increase motor neuron survival. Exp Neurol, 173(1): 46–62

Benes F M, Berretta S (2001). GABAergic interneurons: implications for understanding schizophrenia and bipolar disorder. Neuropsychopharmacology, 25(1): 1–27

Berbari N F, Lewis J S, Bishop G A, Askwith C C, Mykytyn K (2008). Bardet-Biedl syndrome proteins are required for the localization of G protein-coupled receptors to primary cilia. Proc Natl Acad Sci USA, 105(11): 4242–4246

Berbari N F, O'Connor A K, Haycraft C J, Yoder B K (2009). The primary cilium as a complex signaling center. Curr Biol, 19(13): R526–R535

Bishop G A, Berbari N F, Lewis J, Mykytyn K (2007). Type III adenylyl cyclase localizes to primary cilia throughout the adult mouse brain. J Comp Neurol, 505(5): 562–571

Breunig J J, Sarkisian M R, Arellano J I, Morozov Y M, Ayoub A E, Sojitra S, Wang B, Flavell R A, Rakic P, Town T (2008). Primary cilia regulate hippocampal neurogenesis by mediating sonic hedgehog signaling. Proc Natl Acad Sci USA, 105(35): 13127–13132

Bruce A J, Boling W, Kindy M S, Peschon J, Kraemer P J, Carpenter M K, Holtsberg F W, Mattson M P (1996). Altered neuronal and microglial responses to excitotoxic and ischemic brain injury in mice lacking TNF receptors. Nat Med, 2(7): 788–794

Buendia B, Bre M H, Griffiths G, Karsenti E (1990). Cytoskeletal control of centrioles movement during the establishment of polarity in Madin-Darby canine kidney cells. J Cell Biol, 110(4): 1123–1135

Busceti C L, Biagioni F, Aronica E, Riozzi B, Storto M, Battaglia G, Giorgi F S, Gradini R, Fornai F, Caricasole A, Nicoletti F, Bruno V (2007). Induction of the Wnt inhibitor, Dickkopf-1, is associated with neurodegeneration related to temporal lobe epilepsy. Epilepsia, 48(4): 694–705

Coyle P (1976). Vascular patterns of the rat hippocampal formation. Exp Neurol, 52(3): 447–458

Curia G, Longo D, Biagini G, Jones R S, Avoli M (2008). The pilocarpine model of temporal lobe epilepsy. J Neurosci Methods, 172(2): 143–157

DeCaen P G, Delling M, Vien T N, Clapham D E (2013). Direct recording and molecular identification of the calcium channel of primary cilia. Nature, 504(7479): 315–318

Dorr A, Sled J G, Kabani N (2007). Three-dimensional cerebral vasculature of the CBA mouse brain: a magnetic resonance imaging and micro computed tomography study. Neuroimage, 35(4): 1409–1423

Dutta R, McDonough J, Chang A, Swamy L, Siu A, Kidd G J, Rudick R, Mirnics K, Trapp B D (2007). Activation of the ciliary neurotrophic factor (CNTF) signalling pathway in cortical neurons of multiple sclerosis patients. Brain, 130(10): 2566–2576

Einstein E B, Patterson C A, Hon B J, Regan K A, Reddi J, Melnikoff D E, Mateer M J, Schulz S, Johnson B N, Tallent M K (2010). Somatostatin signaling in neuronal cilia is critical for object recognition memory. J Neurosci, 30(12): 4306–4314

Fuchs J L, Schwark H D (2004). Neuronal primary cilia: a review. Cell Biol Int, 28(2): 111–118

Garcia J H, Yoshida Y, Chen H, Li Y, Zhang Z G, Lian J, Chen S, Chopp M (1993). Progression from ischemic injury to infarct following middle cerebral artery occlusion in the rat. Am J Pathol, 142: 623–635

Goetz S C, Anderson K V (2010). The primary cilium: a signalling centre during vertebrate development. Nat Rev Genet, 11(5): 331–344

Han Y G, Alvarez-Buylla A (2010). Role of primary cilia in brain development and cancer. Curr Opin Neurobiol, 20(1): 58–67

Han Y G, Spassky N, Romaguera-Ros M, Garcia-Verdugo J M, Aguilar A, Schneider-Maunoury S, Alvarez-Buylla A (2008). Hedgehog signaling and primary cilia are required for the formation of adult neural stem cells. Nat Neurosci, 11(3): 277–284

Handel M, Schulz S, Stanarius A, Schreff M, Erdtmann-Vourliotis M, Schmidt H, Wolf G, Hollt V (1999). Selective targeting of somatostatin receptor 3 to neuronal cilia. Neuroscience, 89(3): 909–926

Huang L T, Yang S N, Liou C W, Hung P L, Lai M C, Wang C L, Wang T J (2002). Pentylenetetrazol-induced recurrent seizures in rat pups: time course on spatial learning and long-term effects. Epilepsia, 43 (6): 567–573

Inose Y, Kato Y, Kitagawa K, Uchiyama S, Shibata N (2015). Activated microglia in ischemic stroke penumbra upregulate MCP-1 and CCR2 expression in response to lysophosphatidylcholine derived from adjacent neurons and astrocytes. Neuropathology, 35(3): 209–223

Irle E, Markowitsch H J (1982). Connections of the hippocampal formation, mamillary bodies, anterior thalamus and cingulate cortex. A retrograde study using horseradish peroxidase in the cat. Exp Brain Res, 47(1): 79–94

Ishikawa H, Marshall W F (2011). Ciliogenesis: building the cell's

antenna. Nat Rev Mol Cell Biol, 12(4): 222–234

Khan A A, Mao X O, Banwait S, DerMardirossian C M, Bokoch G M, Jin K, Greenberg D A (2008). Regulation of hypoxic neuronal death signaling by neuroglobin. FASEB J, 22(6): 1737–1747

Kumamoto N, Gu Y, Wang J, Janoschka S, Takemaru K, Levine J, Ge S (2012). A role for primary cilia in glutamatergic synaptic integration of adult-born neurons. Nat Neurosci, 15: 399–405, S391

Lee J E, Gleeson J G (2011). Cilia in the nervous system: linking cilia function and neurodevelopmental disorders. Curr Opin Neurol, 24 (2): 98–105

Madsen T M, Newton S S, Eaton M E, Russell D S, Duman R S (2003). Chronic electroconvulsive seizure up-regulates beta-catenin expression in rat hippocampus: role in adult neurogenesis. Biol Psychiatry, 54(10): 1006–1014

Maguschak K A, Ressler K J (2012). The dynamic role of beta-catenin in synaptic plasticity. Neuropharmacology, 62(1): 78–88

Marchi N, Oby E, Batra A, Uva L, De Curtis M, Hernandez N, Van Boxel-Dezaire A, Najm I, Janigro D (2007). *In vivo* and *in vitro* effects of pilocarpine: relevance to ictogenesis. Epilepsia, 48(10): 1934–1946

Massinen S, Hokkanen M E, Matsson H, Tammimies K, Tapia-Paez I, Dahlstrom-Heuser V, Kuja-Panula J, Burghoorn J, Jeppsson K E, Swoboda P, Peyrard-Janvid M, Toftgård R, Castrén E, Kere J (2011). Increased expression of the dyslexia candidate gene DCDC2 affects length and signaling of primary cilia in neurons. PLoS One, 6(6): e20580

Ota A, Ikeda T, Ikenoue T, Toshimori K (1997). Sequence of neuronal responses assessed by immunohistochemistry in the newborn rat brain after hypoxia-ischemia. Am J Obstet Gynecol, 177(3): 519–526

Pan W X, Mao T, Dudman J T (2010). Inputs to the dorsal striatum of the mouse reflect the parallel circuit architecture of the forebrain. Front Neuroanat, 4: 147

Parent J M, Elliott R C, Pleasure S J, Barbaro N M, Lowenstein D H (2006). Aberrant seizure-induced neurogenesis in experimental temporal lobe epilepsy. Ann Neurol, 59(1): 81–91

Parker A K, Le M M, Smith T S, Hoang-Minh L B, Atkinson E W, Ugartemendia G, Semple-Rowland S, Coleman J E, Sarkisian M R (2016). Neonatal seizures induced by pentylenetetrazol or kainic acid disrupt primary cilia growth on developing mouse cortical neurons. Exp Neurol, 282: 119–127

Pedersen L B, Rosenbaum J L (2008). Intraflagellar transport (IFT) role in ciliary assembly, resorption and signalling. Curr Top Dev Biol, 85: 23–61

Pessoa D, Cruz R, Machado B, Tenorio B, Nogueira R (2016). Analysis of electrocorticographic patterns in rats fed standard or hyperlipidic diets in a normal state or during status epilepticus. Nutr Neurosci, 19 (5): 206–212

Quinlan R J, Tobin J L, Beales P L (2008). Modeling ciliopathies: Primary cilia in development and disease. Curr Top Dev Biol, 84: 249–310

Rhee S, Kirschen G W, Gu Y, Ge S (2016). Depletion of primary cilia from mature dentate granule cells impairs hippocampus-dependent contextual memory. Sci Rep, 6: 34370

Rowley S, Liang L P, Fulton R, Shimizu T, Day B, Patel M (2015). Mitochondrial respiration deficits driven by reactive oxygen species in experimental temporal lobe epilepsy. Neurobiol Dis, 75: 151–158

Sierra A, Martin-Suarez S, Valcarcel-Martin R, Pascual-Brazo J, Aelvoet S A, Abiega O, Deudero J J, Brewster A L, Bernales I, Anderson A E, Baekelandt V, Maletić-Savatić M, Encinas J M (2015). Neuronal hyperactivity accelerates depletion of neural stem cells and impairs hippocampal neurogenesis. Cell Stem Cell, 16(5): 488–503

Singla V, Reiter J F (2006). The primary cilium as the cell's antenna: signaling at a sensory organelle. Science, 313(5787): 629–633

Spruston N (2008). Pyramidal neurons: dendritic structure and synaptic integration. Nat Rev Neurosci, 9(3): 206–221

Theilhaber J, Rakhade S N, Sudhalter J, Kothari N, Klein P, Pollard J, Jensen F E (2013). Gene expression profiling of a hypoxic seizure model of epilepsy suggests a role for mTOR and Wnt signaling in epileptogenesis. PLoS One, 8(9): e74428

Valente E M, Rosti R O, Gibbs E, Gleeson J G (2014). Primary cilia in neurodevelopmental disorders. Nat Rev Neurol, 10(1): 27–36

Wang Z, Phan T, Storm D R (2011). The type 3 adenylyl cyclase is required for novel object learning and extinction of contextual memory: role of cAMP signaling in primary cilia. J Neurosci, 31(15): 5557–5561

Ware S M, Aygun M G, Hildebrandt F (2011). Spectrum of clinical diseases caused by disorders of primary cilia. Proc Am Thorac Soc, 8 (5): 444–450

Winter C G, Saotome Y, Levison S W, Hirsh D (1995). A role for ciliary neurotrophic factor as an inducer of reactive gliosis, the glial response to central nervous system injury. Proc Natl Acad Sci USA, 92(13): 5865–5869

Wolf H K, Buslei R, Schmidt-Kastner R, Schmidt-Kastner P K, Pietsch T, Wiestler O D, Blumcke I (1996). NeuN: a useful neuronal marker for diagnostic histopathology. J Histochem Cytochem, 44(10): 1167–1171

Yagita Y, Kitagawa K, Ohtsuki T, Takasawa K, Miyata T, Okano H, Hori M, Matsumoto M (2001). Neurogenesis by progenitor cells in the ischemic adult rat hippocampus. Stroke, 32(8): 1890–1896

Yin Y, Zhao X, Fang Y, Huang L (2010). Carotid artery wire injury mouse model with a nonmicrosurgical procedure. Vascular, 18(4): 221–226

Yoder B K (2007). Role of primary cilia in the pathogenesis of polycystic kidney disease. J Am Soc Nephrol, 18(5): 1381–1388

Zhao C, Teng E M, Summers R G Jr, Ming G L, Gage F H (2006). Distinct morphological stages of dentate granule neuron maturation in the adult mouse hippocampus. J Neurosci, 26(1): 3–11